Journal of Magnetic Resonance 214 (2012) 81–90

Contents lists available at SciVerse ScienceDirect

Journal of Magnetic Resonance

journal homepage: www.elsevier.com/locate/jmr

A comparison of NCO and NCA transfer methods for biological solid-state NMR spectroscopy

Nikolaus M. Loening [a,b,*], Morten Bjerring [c], Niels Chr. Nielsen [c], Hartmut Oschkinat [b]

[a] Department of Chemistry, Lewis & Clark College, 0615 SW Palatine Hill Road, Portland, OR 97219, USA
[b] Leibniz-Institut für Molekulare Pharmakologie (FMP), Robert-Rössle-Strasse 10, 13125 Berlin, Germany
[c] Center for Insoluble Protein Structures (inSPIN), Interdisciplinary Nanoscience Center (iNANO) and Department of Chemistry, Aarhus University, DK-8000 Aarhus C, Denmark

ARTICLE INFO

Article history:
Received 13 August 2011
Revised 24 September 2011
Available online 2 November 2011

Keywords:
Dipolar recoupling
NCO
NCA
Optimal control

ABSTRACT

Three different techniques (adiabatic passage Hartman-Hahn cross-polarization, optimal control designed pulses, and EXPORT) are compared for transferring ^{15}N magnetization to ^{13}C in solid-state NMR experiments under magic-angle-spinning conditions. We demonstrate that, in comparison to adiabatic passage Hartman-Hahn cross-polarization, optimal control transfer pulses achieve similar or better transfer efficiencies for uniformly-^{13}C,^{15}N labeled samples and are generally superior for samples with non-uniform labeling schemes (such as 1,3- and 2-^{13}C glycerol labeling). In addition, the optimal control pulses typically use substantially lower average RF field strengths and are more robust with respect to experimental variation and RF inhomogeneity. Consequently, they are better suited for demanding samples.

1. Introduction

The efficient transfer of magnetization from amide nitrogens (N) to alpha (C_α) or carbonyl (C_o) carbons is essential for a variety of biological NMR experiments. For solid-state samples under magic-angle-spinning (MAS) conditions, this transfer can be carried out by recoupling the dipolar interaction using techniques such as double cross-polarization (DCP) and its variants [1–5], symmetry-based recoupling [6–8], pulses designed using optimal control (OC) [9,10], or multiple-oscillating field techniques such as EXPORT [11].

Despite the variety of sequences that can be used for N to C_α (NCA) and N to C_o (NCO) magnetization transfer, the current standard sequence used in most laboratories is the adiabatic passage Hartmann-Hahn cross-polarization experiment [3] (which we refer to in the following as adiabatic DCP). In adiabatic DCP, the amplitude of one RF channel is held constant while the amplitude of the other channel is adiabatically modulated. This sequence has the advantage that complete magnetization transfer is theoretically possible (i.e., a transfer efficiency of 100%) but has the disadvantages of demanding a relatively long duration of strong RF irradiation and a relatively narrow match condition for the RF amplitude. Consequently, the performance of adiabatic DCP is quite sensitive to calibration, the homogeneity of the RF field, and the stability of the instrument. In practice, signal loss due to relaxation as well as RF heating of the sample limits the length of the cross-polarization period and, therefore, the experimental transfer efficiency.

In this paper, we compare the NCA and NCO transfer efficiencies for adiabatic DCP with two more recently introduced magnetization transfer methods: transfer pulses designed using optimal control transfer pulses (^{OC}DCP) [9,10] and the EXPORT sequence [11]. Optimal control theory [12,13] is an efficient method for simultaneously optimizing hundreds, or even thousands, of variables to maximize a desired outcome. In the context of NMR spectroscopy, the variables are usually the amplitudes and phases of the RF field, and the outcome is the transfer efficiency from one state to another [14]. The main strength of optimal control is that all of the variables are adjusted in each iteration of the calculation, thereby making it possible for a calculation with a huge number of variables to converge in a reasonable amount of computation time.

The EXPORT sequence is a recent development in ^{15}N–^{13}C transfer methods [11], which, under certain conditions, is able to transfer magnetization without the need for simultaneous ^{1}H decoupling. Whereas magnetization is spin-locked in an adiabatic DCP transfer, in an EXPORT transfer the magnetization is predominantly perpendicular to the RF field. The conditions under which it is possible to use EXPORT without decoupling are quite demanding for the ^{13}C and ^{15}N channels, but it is also possible to use lower-power match conditions (along with simultaneous ^{1}H decoupling) for NCA and NCO transfers, which will be the variant explored in this paper.

In the following, we will show that under the conditions investigated, adiabatic DCP and ^{OC}DCP tend to have similar efficiencies

* Corresponding author at: Department of Chemistry, Lewis & Clark College, 0615 SW Palatine Hill Road, Portland, OR 97219, USA. Fax: +1 503 768 7369.
E-mail address: loening@lclark.edu (N.M. Loening).

1090-7807/$ - see front matter © 2011 Elsevier Inc. All rights reserved.
doi:10.1016/j.jmr.2011.10.012

for ^{15}N–^{13}C transfers for uniformly-labeled samples. For samples with non-uniform labeling (such as 1,3- and 2-^{13}C glycerol labeling), ^{OC}DCP has significantly higher transfer efficiencies than adiabatic DCP. In all cases ^{OC}DCP has the advantages of being more tolerant of inhomogeneities of the RF field, being less sensitive to calibration, and requiring less RF power than the other two methods.

2. Experimental

2.1. Simulations

All simulations were performed using SIMPSON 3.0.1 [15,16]. The source code and compiled binaries for this program are freely available for download at http://www.bionmr.chem.au.dk/bionmr/software/simpson.php. The simulations used 20 REPULSION [17] α, β crystallite angles and 5 γ angles for powder averaging. Calculations with larger sets of crystallites produced results that were essentially the same but at the expense of increased computation time.

2.2. Adiabatic DCP

Adiabatic passage Hartman-Hahn cross-polarization (adiabatic DCP) was performed using a constant RF amplitude for the ^{15}N channel (ν_{RF}^{N}) and an adiabatic amplitude ramp for the ^{13}C channel (ν_{RF}^{C}). The match condition for Hartman-Hahn transfer under magic-angle spinning conditions is that the amplitudes of the two RF fields differ by one or two times the spinning frequency. In practice, we usually set the RF amplitudes to be half-integer multiples of the spinning frequency in order to avoid hitting R^3 conditions. For NCA transfers, the $\nu_{RF}^{N} = \frac{5}{2}\nu_r,\ \nu_{RF}^{C} = \frac{3}{2}\nu_r$ match condition was used (where ν_r is the spinning frequency in Hz). In the experiments presented, ν_r = 14 kHz so the corresponding average RF field strengths were 35 kHz for ^{15}N and 21 kHz for ^{13}C. Experimentally, we found that the optimal adiabatic DCP length for NCA transfers was between 4 and 5 ms for our samples.

For NCO experiments, the $\nu_{RF}^{N} = \frac{3}{2}\nu_r,\ \nu_{RF}^{C} = \frac{5}{2}\nu_r$ match condition was used, which we found for our samples to have a higher experimental transfer efficiency than the more typical $\nu_{RF}^{N} = \frac{5}{2}\nu_r$, $\nu_{RF}^{C} = \frac{7}{2}\nu_r$ NCO match condition. The corresponding average RF field strengths were 21 kHz for ^{15}N and 35 kHz for ^{13}C. For the samples investigated, the transfer efficiency tended to plateau for cross-polarization periods longer than 5 ms.

Other match conditions were investigated for both NCA and NCO transfers, but these had lower experimental transfer efficiencies. The pulse shapes used for adiabatic DCP are illustrated in the first column of Fig. 1. For simulations, the same NCA match condition was used as in our experiments ($\nu_{RF}^{N} = \frac{5}{2}\nu_r,\ \nu_{RF}^{C} = \frac{3}{2}\nu_r$) but for simulations of NCO transfers the $\nu_{RF}^{N} = \frac{5}{2}\nu_r,\ \nu_{RF}^{C} = \frac{7}{2}\nu_r$ condition was used as this match condition has better theoretical performance.

The pulse shapes used for adiabatic DCP along with the parameters used to generate them are provided with the Supplementary materials.

2.3. ^{OC}DCP

We generated optimal control transfer pulses using the optimal control procedures [16] included in SIMPSON 3.0.1 [15]. As with the simulations, the optimizations used 20 REPULSION α, β crystallite angles and 5 γ angles for powder averaging. Although it is possible to generate ^{OC}DCP pulses including all of the parameters to be optimized from the start of the calculation, we found that the optimizations were less time consuming if broken into a series of steps. Typically, the optimal control pulses were calculated in three or four steps, where the best pulses from each step were used as input for the subsequent step of the calculation. The parameters included in each step of the calculation were:

1. A narrow-band optimization for ^{15}N to ^{13}C transfer. The tensor values for the nuclear spin interactions are given in Table 1 [10] and the isotropic chemical shifts were set to 0 (i.e., all pulses are designed to work with the transmitter on resonance with the relevant nuclei).
2. Chemical shift offsets were added to ensure transfer over the desired chemical shift range (four points over 40 ppm for N, five points over 25 ppm for C_α, three points over 15 ppm for C_o).
3. An RF inhomogeneity profile was added. The profile used was a 8% Gaussian (full-width-half-height for the RF profile relative to the nominal RF field strength) with five points for each channel (0.9, 0.95, 1.0, 1.05, and 1.1 times the nominal field strength).
4. For NCA transfers, two CSA values ($\delta_{aniso} = -20$, 20 ppm) and two asymmetry values ($\eta = 0.4, 0.9$) were used in the optimization.

The overall pulse length, the length of the steps within the pulse, the spinning frequency, and the magnetic field all need to be specified at the beginning of the calculation. Overall pulse lengths between 1 and 5 ms were investigated. In all cases, the time steps within the pulses were set to 10 μs (so, for example, a 2 ms pulse consists of 200 elements for each channel). Pulses were calculated for a spinning frequency of 12 kHz with a 14.1 T magnetic field (600 MHz for ^1H) or with a spinning frequency of 14 kHz with a 16.4 T magnetic field (700 MHz for ^1H). Only data for the 700 MHz pulses are shown, as the performance of the 600 MHz pulses was similar. Shape files for both spinning frequencies/fields are provided in the Supplementary information as well as at http://www.lclark.edu/~loening/pulses.html. Although the pulses were designed to transfer magnetization from ^{15}N (initial operator: I_x) to ^{13}C (destination operator: S_x), the opposite transfer (from ^{13}C to ^{15}N) can be performed simply by time-reversing the pulses. The transfer efficiencies of the reversed pulses are typically within 10% of the original transfer efficiencies.

Typically, five to ten ^{OC}DCP pulses were calculated for each set of conditions (magnetic field, pulse length, spinning frequency). Each calculation was initialized with a pulse with random amplitudes and phases, and with an initial maximum RF amplitude of 10 kHz. In the calculation, the maximum allowed RF amplitude was limited to 50 kHz for each channel. In some calculations, the maximum RF amplitude was reduced to 25 kHz for ^{15}N and limited to be between 11 and 17 kHz for ^{13}C (for NCA transfers) or between 4 and 17 kHz for ^{13}C (for NCO transfers). These pulses had similar performance (and similar average RF amplitudes) as the pulses calculated with the higher maximum RF amplitude.

The optimal control pulses were tested to select the ones that had the highest transfer efficiencies under experimental conditions. Interestingly, the experimental results did not always correlate with the simulated transfer efficiencies. In most cases, the differences between the theoretical and experimental transfer efficiencies are largely due to how the pulses behave in multiple-spin systems (see below). Examples of the best 2 ms NCA and NCO ^{OC}DCP pulses for use at 700 MHz for ^1H and with a spinning frequency of 14 kHz are shown in the second column of Fig. 1. For samples with non-uniform ^{13}C-labeling, we found that 3 ms ^{OC}DCP pulses performed better than 2 ms pulses.

2.4. EXPORT

The conditions under which it is possible to use EXPORT without decoupling are quite demanding experimentally; typically

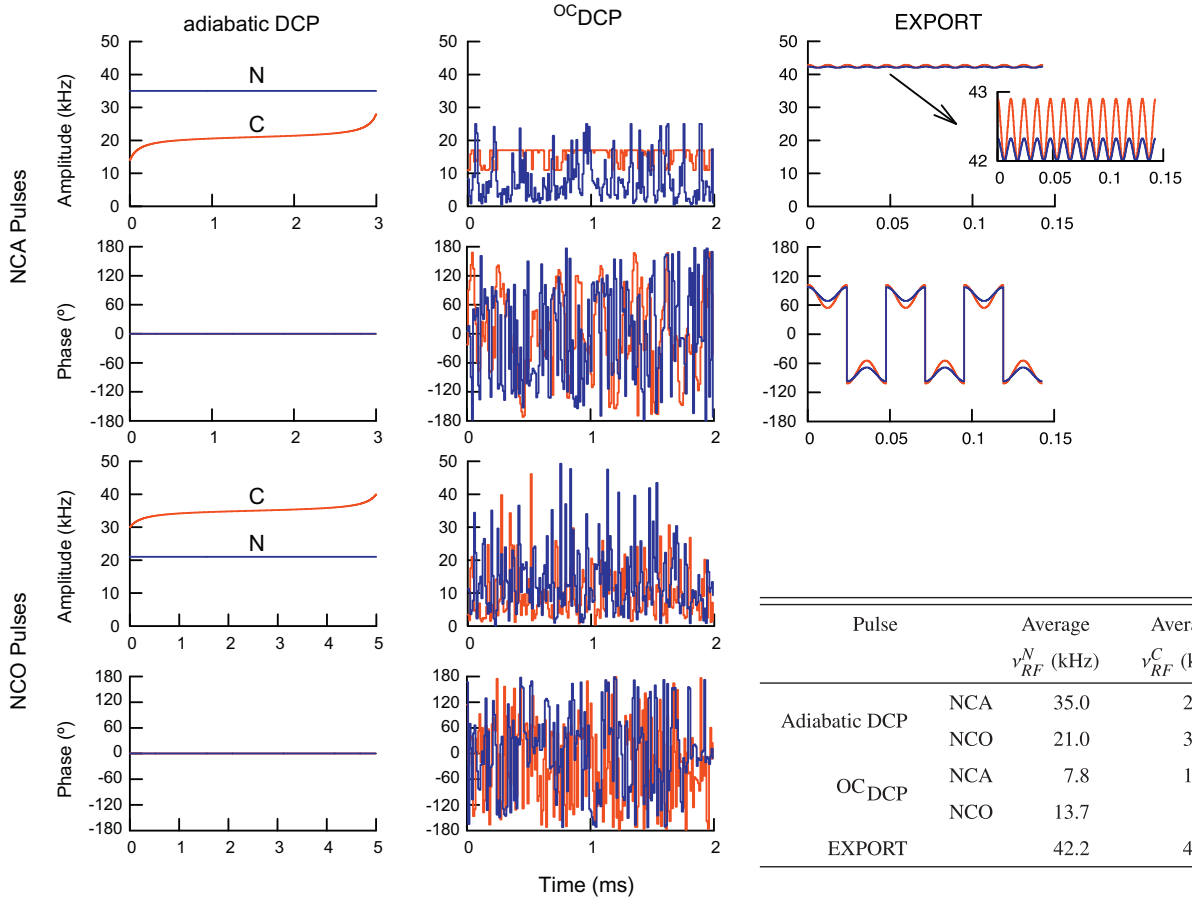

Pulse		Average ν^{N}_{RF} (kHz)	Average ν^{C}_{RF} (kHz)
Adiabatic DCP	NCA	35.0	21.0
	NCO	21.0	35.0
OCDCP	NCA	7.8	15.3
	NCO	13.7	9.6
EXPORT		42.2	42.5

Fig. 1. Amplitude and phase profiles for the ^{15}N–^{13}C transfer pulses used in this paper for experiments at 700 MHz for ^{1}H with ν_r = 14 kHz. The inset table provides the average RF amplitude (in kHz) for each channel of each pulse. Data are shown in blue for the ^{15}N channel and in red for the ^{13}C channel. Adiabatic DCP is only amplitude modulated (phase is set to 0° for both channels). For EXPORT, the same sequence is used for both NCA and NCO transfers with only a change in the carrier frequency. In addition, for EXPORT only the basic building block (which is two rotor cycles long) is shown; the number of times that this block was repeated was experimentally optimized for each sample to maximize transfer efficiency. (For interpretation of the references to color in this figure legend, the reader is referred to the web version of this article.)

Table 1
Chemical shielding, *J*, and dipolar coupling tensor values used for OC pulse design and simulations. Definitions of parameters can be found in Bak et al. [18].

Nucleus	CSA, δ_{aniso} (ppm)	Asymmetry, η	Euler angles (°) α_{PC}	β_{PC}	γ_{PC}
N	99	0.19	−90	−90	17
C_α	−20	0.43	90	90	0
C_o	−76	0.90	0	0	94

Interaction	Coupling constant (Hz)	Euler angles (°) α_{PC}	β_{PC}	γ_{PC}
NC_α dipolar ($b/2\pi$)	890	90	115.3	0
NC_o dipolar ($b/2\pi$)	1176	0	90	57
NC_α scalar (J)	−11			
NC_o scalar (J)	−15			

70–80 kHz RF amplitudes are required simultaneously on both the ^{13}C and the ^{15}N channels in order to be able to use this sequence without ^{1}H decoupling [11]. As our 3.2 and 4 mm probes are not able to generate these RF amplitudes, we used a lower power match conditions for EXPORT. In our case, we used the $C/2\pi = 3\nu_r$, $B_I/2\pi = 3\nu_r/8$, and $B_S/2\pi = 5\nu_r/8$ condition, where $C/2\pi$ represents the amplitude of the RF field along the *y*-axis for both channels, and $B_I/2\pi$ and $B_S/2\pi$ represent the amplitudes of the ^{15}N and ^{13}C RF fields along the *x*-axis. The EXPORT building block for these conditions and ν_r = 14 kHz is illustrated in the third column of Fig. 1. This building block is repeated every two rotor cycles, and the number of repetitions was experimentally determined for each sample. For NCA transfers, the maximum transfer efficiency was typically achieved with 18 repetitions (2.57 ms) and, for NCO transfers, with between 14 and 19 repetitions (2.0–2.7 ms).

2.5. Samples

Samples of the α-spectrin SH3 domain were prepared as described previously [19]. Briefly, the SH3 domain was expressed in *Escherichia coli* using M9 minimal media supplemented with ^{15}N-labeled NH_4Cl and either [U–^{13}C]-labeled glucose or [2-^{13}C]-labeled glycerol. The sample was purified by anion exchange chromatography, gel filtration, and dialysis, and then precipitated by changing the pH. The precipitate was separated by centrifugation, after which approximately 5–10 mg of protein precipitate was packed into a 3.2 mm sample rotor. A top spacer was used in each sample to confine the sample to the center of the rotor.

The [1,3-^{13}C,U–^{15}N]-labeled OmpG sample was expressed and prepared as described previously [20]. In brief, the cells were predominately grown on unlabeled rich medium and then transferred into M9 minimal medium containing [1,3-^{13}C]-labeled glycerol and ^{15}N-labeled NH_4Cl. After 1 h of incubation, protein expression was induced and the cells were harvested after 3 h. The protein was purified under denaturing conditions, refolded in a detergent

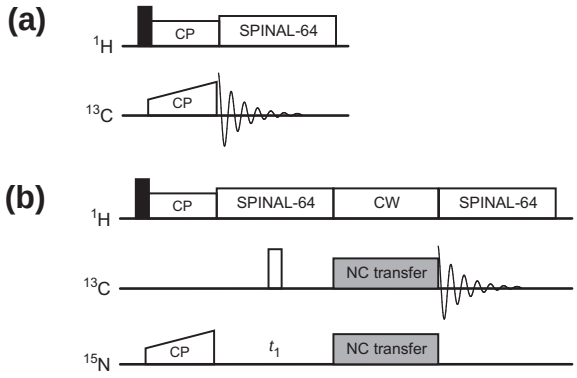

Fig. 2. The ^{13}C CP-MAS experiment (a) and the NCA/NCO experiment (b). The "NC transfer" period was switched between adiabatic DCP, ^{OC}DCP, and the EXPORT sequence. Filled and open rectangles represent excitation (90°) and refocusing (180°) pulses, respectively.

containing buffer, reconstituted into *E. coli* lipids, and crystallized by dialysis before packing ≈10 mg of sample material into a 3.2 mm rotor.

2.6. NMR Experiments

The sample temperature was maintained at 275 K for all experiments.

Continuous wave and SPINAL-64 [21] ^{1}H decoupling were used during pulses and delays, respectively, with a decoupling field strength of ∼85 kHz. At lower decoupling field strengths the ^{15}N–^{13}C transfer efficiencies began to decrease, whereas higher strength decoupling (100–120 kHz) resulted in negligible improvements to the observed ^{15}N–^{13}C transfer efficiencies.

The ^{15}N–^{13}C transfer pulses were tested on a Bruker (Rheinstetten, Germany) Avance 600 MHz (14.1 T) spectrometer using 3.2 mm and 4 mm HXY MAS probes and on a Bruker Avance 700 MHz (16.4 T) spectrometer using a 3.2 mm HXY MAS probe. The MAS frequency (ν_r) was set to 12 kHz for experiments on the 600 MHz spectrometer and 14 kHz for experiments on the 700 MHz spectrometer. One-dimensional spectra were acquired with 32 scans and a 3 s recycle delay. The linearity of the RF amplifiers for both spectrometers was calibrated and tested using the "CORTAB" procedure included in the Bruker spectrometer software.

For the NCO and NCA experiments (Fig. 2b), the first step was a CP-MAS transfer from ^{1}H to ^{15}N. For this transfer, a constant ^{1}H RF amplitude of ≈65 kHz was used along with a linear ramp from 30 to 60 kHz of the ^{15}N RF field. The optimized contact time was 1.5 ms. Immediately after the CP step, the magnetization was transferred from ^{15}N to ^{13}C using one of the three transfer methods previously mentioned. Selective transfer was achieved by setting the carrier frequency to be on-resonance with either C_o or C_α during the transfer period. For all transfer pulses, a two-dimensional grid search was used to optimize the power level of the ^{13}C and ^{15}N channels prior to use. The length of the adiabatic DCP period and the number of EXPORT cycles were also experimentally optimized for each sample and experiment.

For comparison, one-dimensional ^{13}C CP-MAS experiments (Fig. 2a) were carried out under conditions optimized for transfer of magnetization to C_o or C_α. In both cases, the ^{1}H RF amplitude was held at a constant value (≈60 kHz) while linearly ramping the ^{13}C RF field from 30 to 60 kHz (for C_α) or from 35 to 75 kHz (for C_o). The ^{13}C RF transmitter was moved to be in the middle of the C_o or C_α region. The contact time was 0.5 ms for CP transfers to C_α and between 2 and 3.5 ms for transfers to C_o.

3. Results

Experimental transfer efficiencies for the SH3 and OmpG samples are shown in Table 2, and the corresponding spectra for some of these experiments are shown in Fig. 3. The ^{15}N–^{13}C transfer efficiencies were measured relative to ^{13}C CP-MAS spectra that were optimized for transfer to C_α or C_o. Although every step of the experiments that generated these results was carefully optimized, these "absolute" transfer efficiencies may be somewhat misleading due to differences in the efficiency of the ^{1}H-^{15}N CP step compared to the ^{1}H–^{13}C CP step in the reference experiments. Nevertheless, the normalized transfer efficiencies between the different methods do not depend on the absolute transfer efficiencies, so any systematic errors in the efficiency of the ^{1}H–^{13}C or ^{1}H-^{15}N CP steps do not affect our conclusions.

In all cases, NCA transfers are less efficient than NCO transfers. This is primarily because alpha carbons relax more quickly than carbonyl carbons during the transfer period, but also because the N–C_α dipolar coupling is weaker than the N–C_o coupling. Faster relaxation of the OmpG membrane protein sample relative to the microcrystalline SH3 samples also explains why the transfer efficiencies for [2-^{13}C,U–^{15}N] SH3 are higher than for [1,3-^{13}C,U–^{15}N] OmpG. The normalized transfer efficiencies clearly show that ^{OC}DCP is comparable or better than adiabatic DCP for uniformly-labeled samples, and clearly outperform adiabatic DCP for [2-^{13}C,U–^{15}N]-labeled and [1,3-^{13}C,U–^{15}N]-labeled samples. The reason for this trend is discussed in the next section.

Fig. 4 illustrates the simulated and experimental buildup curves for the three transfer sequences. For ^{OC}DCP, discrete points are shown as multiple pulses were calculated for each pulse length; the graph shows the results from a large number of pulses for which only the ones that performed best under experimental conditions were used for both the simulated and experimental results in this paper. For ^{OC}DCP, the experimental transfer efficiencies are below their theoretical values, an observation that will be discussed further in the next section.

Table 2
Experimental efficiencies for the ^{15}N-^{13}C transfer methods. Transfer efficiencies were measured relative to ^{13}C CP-MAS spectra that were optimized for either C_o or C_α. The percentage values were determined by scaling the spectra to the same height rather than by integration. For normalized transfer efficiencies, the adiabatic DCP transfer efficiency is set to 100%, and the other transfer efficiencies scaled accordingly.

Experiment	Sample	Transfer efficiencies (%)			Normalized transfer efficiencies (%)		
		Adiabatic DCP	^{OC}DCP	EXPORT	Adiabatic DCP	^{OC}DCP	EXPORT
NCA	[U–^{13}C,U–^{15}N] SH3	26	26	16	100	100	62
	[2-^{13}C,U–^{15}N] SH3	37	47	26	100	127	70
	[1,3-^{13}C,U–^{15}N] OmpG	26	37	14	100	142	54
NCO	[U–^{13}C,U–^{15}N] SH3	56	61	32	100	109	57
	[2-^{13}C,U–^{15}N] SH3	46	52	32	100	113	70
	[1,3-^{13}C,U–^{15}N] OmpG	35	47	25	100	134	71

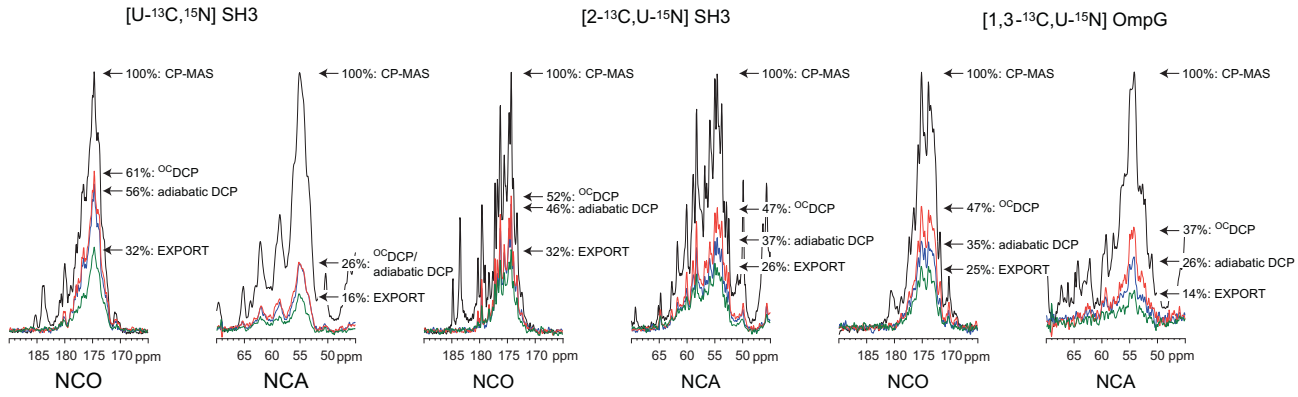

Fig. 3. Representative 1D ^{13}C solid-state NMR spectra illustrating the transfer efficiencies of adiabatic DCP, ^{OC}DCP, and EXPORT in comparison to ^{13}C CP-MAS spectra (pulse sequences are shown in Fig. 2). The percentages are the same as in Table 2. Spectra were acquired at 700 MHz for ^{1}H and with $\nu_r = 14$ kHz. The ^{13}C CP-MAS spectra were optimized for either C_o or C_α.

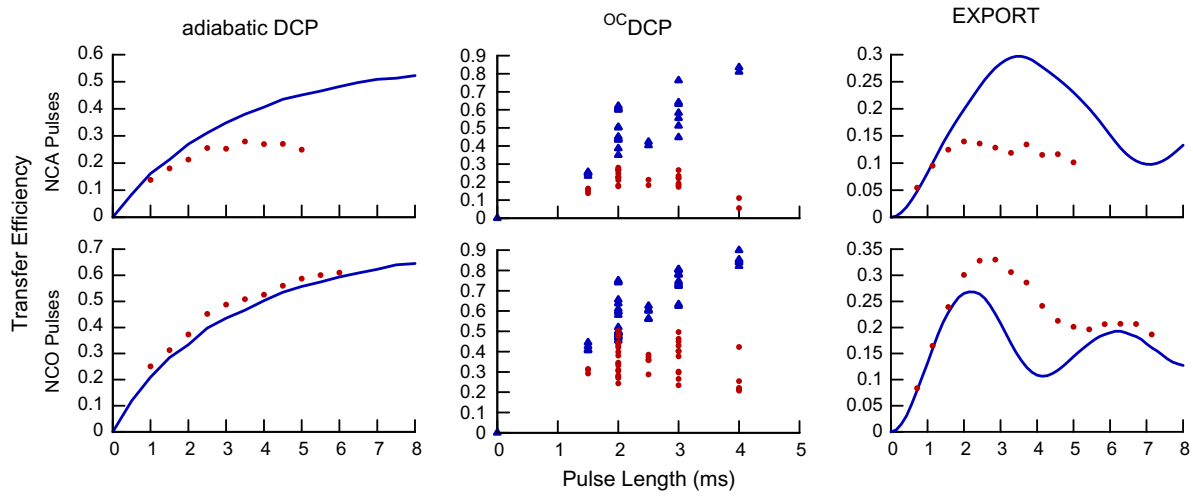

Fig. 4. Simulated and experimental NCA and NCO transfer efficiencies for adiabatic DCP, ^{OC}DCP, and EXPORT as a function of pulse length at 700 MHz for ^{1}H and with $\nu_r = 14$ kHz. The blue lines (or blue triangles) represent simulation results and the red circles represent experimental results. As ^{OC}DCP pulses cannot be varied in length, a number of different pulses with pulse lengths between 1.5 and 4 ms were calculated and then simulated (blue triangles). The simulations used a ^{13}C–^{15}N two-spin system and a 8% gaussian RF inhomogeneity profile. The experimental results were acquired using a [U–^{13}C,U–^{15}N] SH3 sample and were measured relative to ^{13}C CP-MAS spectra that were optimized for transfer to C_α or C_o. (For interpretation of the references to color in this figure legend, the reader is referred to the web version of this article.)

The simulated transfer efficiency as a function of chemical shift offsets is shown in Fig. 5. All three transfer methods are able to cover the required range of chemical shifts for NCA and NCO transfers. ^{OC}DCP pulses have relatively uniform transfer efficiencies over the required range (40 ppm for amides, 25 ppm for C_α, 15 ppm for C_o) but rapidly drop off at larger offsets, whereas adiabatic DCP and EXPORT transfers have broader profiles. In some situations, this is an advantage for ^{OC}DCP, as it allows for much cleaner selection of different spectral regions. Note that in this figure (as in Figs. 6 and 7) the transfer efficiency is normalized such that the maximum transfer efficiency is set to 1.0 for each graph. This is to make it easier to compare the performance of the methods for a given parameter; transfer efficiencies relative to ^{13}C CP-MAS spectra are provided in Figs. 3 and 4, as well as Table 2.

Both simulated and experimental transfer efficiencies for the three methods as a function of the RF field strengths are shown in Fig. 6. For adiabatic DCP, RF field amplitude variations of 1–2% on either channel results in a large decrease in transfer efficiency. The only situation where adiabatic DCP can tolerate RF inhomogeneities is if the variation between the two channels is positively correlated. EXPORT behaves somewhat better than adiabatic DCP with respect to RF inhomogeneities, particularly for NCO transfers where the large ^{13}C CSA broadens the match condition. For small variations in the RF homogeneity (±10%), EXPORT deals well with a negative correlation between the channels. Of the three transfer methods, ^{OC}DCP deals the best with RF inhomogeneities. It can tolerate variations of 5–10% in the RF amplitude before a major decrease in transfer efficiency occurs, even if the homogeneities of the channels are not correlated (hence the relatively "square" RF profile in Fig. 6). The greater tolerance of ^{OC}DCP to variations in the RF amplitude not only makes these pulses easier to calibrate and more robust to instrumental drift, but also results in higher signal levels under experimental conditions. This is because the broader match condition of ^{OC}DCP compensates for inhomogeneities in the RF field. Consequently, more of the sample volume is able to contribute to the NMR signal.

4. Discussion

4.1. Adiabatic DCP

As mentioned in the introduction, adiabatic DCP is the current standard for ^{15}N–^{13}C magnetization transfer in solid-state NMR

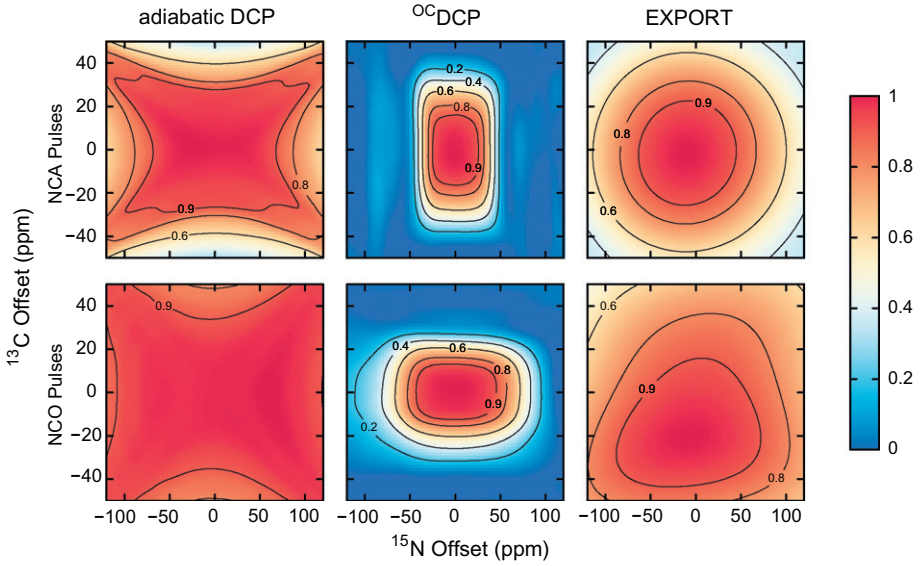

Fig. 5. Simulated NCA and NCO normalized transfer efficiencies for adiabatic DCP, ^{OC}DCP, and EXPORT as a function of ^{15}N and ^{13}C chemical shift offset at 700 MHz for ^{1}H and with ν_r = 14 kHz. Although ^{OC}DCP pulses cover a much narrower range of offsets than the other two transfer methods, the range is more than adequate for the range of offsets expected for C_o, C_α, and N resonances in biological samples. The well-defined chemical shift offset range of the ^{OC}DCP pulses should result in cleaner selection of different regions of the spectrum than the other two methods, which can be an advantage is some situations. The simulations use a ^{13}C–^{15}N two-spin system and a 8% gaussian RF inhomogeneity profile. The transfer efficiencies are normalized such that, for each graph, the maximum transfer efficiency is set to 1.0. The normalization scale factors (i.e., the maximum absolute transfer efficiency) for NCA simulations were 0.35, 0.59, and 0.32 for adiabatic DCP, ^{OC}DCP, and EXPORT, respectively and for NCO simulations were 0.56, 0.66, and 0.28 for adiabatic DCP, ^{OC}DCP, and EXPORT, respectively.

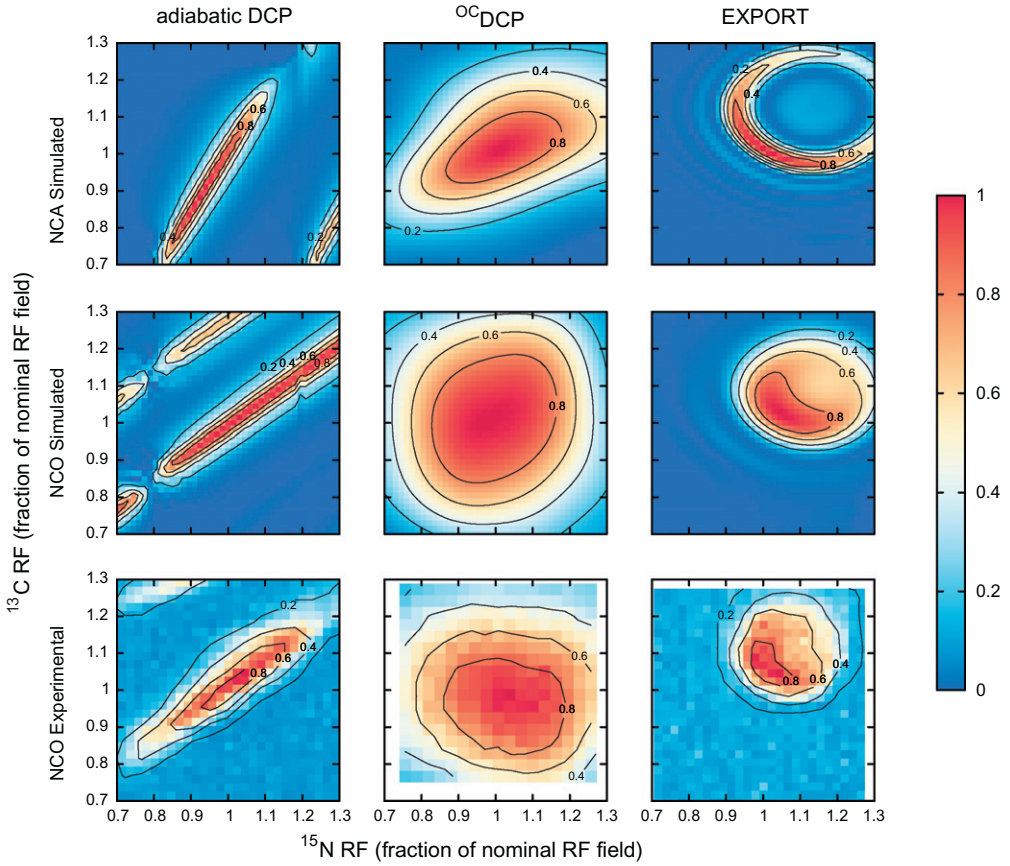

Fig. 6. Simulated and experimental NCA and NCO normalized transfer efficiencies for adiabatic DCP, ^{OC}DCP, and EXPORT as a function of ^{15}N and ^{13}C RF field strengths at 700 MHz for ^{1}H and with ν_r = 14 kHz. The horizontal and vertical axes are given in terms of the fraction of the nominal RF field strength; the absolute RF fields (corresponding to 1.0) are given in the inset table in Fig. 1. The simulations use a ^{13}C–^{15}N two-spin system. The transfer efficiencies are normalized such that, for each graph, the maximum transfer efficiency is set to 1.0. The normalization scale factors (i.e., the maximum absolute transfer efficiency) for NCA simulations were 0.50, 0.59, and 0.73 for adiabatic DCP, ^{OC}DCP, and EXPORT, respectively and for NCO simulations were 0.66, 0.68, and 0.50 for adiabatic DCP, ^{OC}DCP, and EXPORT, respectively. The experimental results were acquired using a [U–^{13}C,U–^{15}N] SH3 sample.

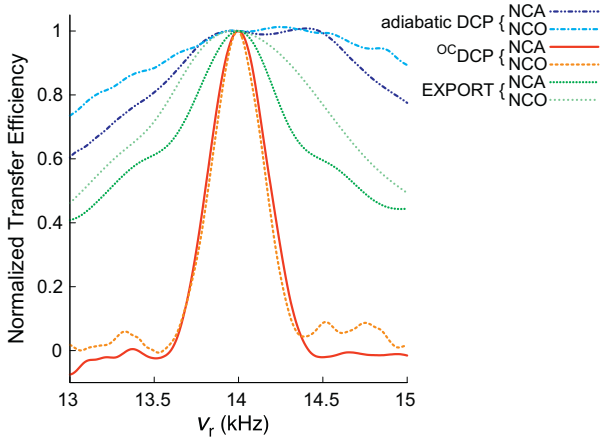

Fig. 7. Simulated NCA and NCO normalized transfer efficiencies for adiabatic DCP, ^{OC}DCP, and EXPORT as a function of spinning frequency at 700 MHz for ^{1}H. The simulations use a ^{13}C–^{15}N two-spin system and a 8% gaussian RF inhomogeneity profile. The transfer efficiency is normalized such that, for each graph, the transfer efficiency at 14 kHz spinning is set to 1.0. The normalization scale factors (i.e., the maximum absolute transfer efficiency) for NCA simulations were 0.35, 0.59, and 0.32 for adiabatic DCP, ^{OC}DCP, and EXPORT, respectively and for NCO simulations were 0.56, 0.66, and 0.28 for adiabatic DCP, ^{OC}DCP, and EXPORT, respectively.

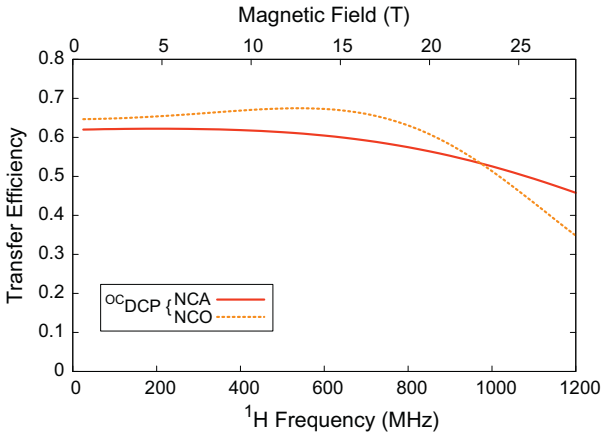

Fig. 8. Simulated on-resonance transfer efficiencies for the NCA and NCO ^{OC}DCP pulses shown in Fig. 1 as a function of ^{1}H frequency/magnetic field. The simulations use a ^{13}C–^{15}N two-spin system, a 8% gaussian RF inhomogeneity profile, and ν_r = 14 kHz.

spectroscopy. In light of the results shown in this paper, adiabatic DCP may still be a good choice in some situations, particularly with uniformly ^{13}C-labeled samples and for systems with very homogeneous RF fields (such as samples with restricted volumes). However, adiabatic DCP does have several drawbacks. First, very high transfer efficiencies (approaching 100%) are theoretically possible but only for very long cross-polarization periods. For most biological samples relaxation limits the cross-polarization period to be between 3 and 8 ms and for samples that relax especially quickly it may be better to use ^{OC}DCP or EXPORT, which tend to reach maximum transfer efficiency in half the time (2–3 ms). In addition, in adiabatic DCP the application of relatively high power RF irradiation for such a long period simultaneously on three channels (including the ^{1}H decoupling) can cause problems with sample heating. The third major drawback is that the match condition for adiabatic DCP is very narrow; optimizing the pulses to get maximum efficiency can be a tedious process and any changes in sample or instrument conditions during the course of an experiment will often change the match condition with a corresponding loss of transfer efficiency.

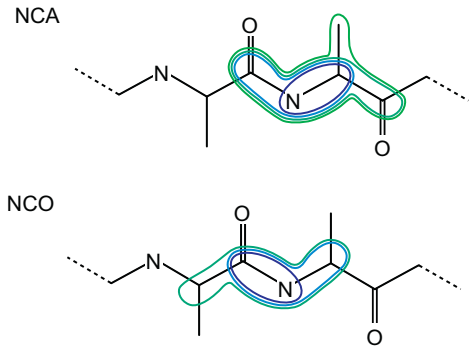

Fig. 9. Topologies used for multiple spin simulations. For NCA experiments systems with up to five spins were used to test the dependence of the transfer methods on neighboring nuclei, whereas for NCO experiments systems with a maximum of four spins were used in the simulations.

4.2. ^{OC}DCP

For uniformly ^{13}C-labeled samples, pulses designed using optimal control theory performed comparably with or even slightly better than adiabatic DCP for NCA and NCO transfers. For sparsely ^{13}C-labeled samples, such as our [2-^{13}C,U–^{15}N] SH3 and [1,3-^{13}C,U–^{15}N] OmpG samples, ^{OC}DCP clearly performs better than adiabatic DCP by 30–40% for NCA transfers and 10–30% for NCO transfers.

Even in situations where ^{OC}DCP only performs as well as (or worse than) adiabatic DCP, it may still be desirable for several reasons. For sensitive samples, ^{OC}DCP allows transfers with much less RF irradiation on the ^{13}C and ^{15}N channels and, for rapidly-relaxing samples, the shorter length for ^{OC}DCP pulses may be advantageous. In addition, for long experiments with unstable spectrometers or sensitive unstable samples, the broader match condition for ^{OC}DCP can be beneficial, as the transfer efficiency will vary less over the course of an experiment than for an adiabatic DCP transfer. Experimentally, ^{OC}DCP is also much quicker to setup as the optimal RF power level is much easier to find. This can be a considerable advantage when working with samples with low sensitivity where optimizing power levels is difficult.

With optimal control, one has to "be careful what you wish for" when designing pulses. Optimal control calculations usually produce pulses that work well for the specific conditions that were used for the optimization, but may or may not be optimal for variables that were unconstrained in the calculation. For example, the optimal control NCA and NCO pulses presented in this paper were optimized to be tolerant of RF inhomogeneity, but were optimized for a single MAS spinning frequency and consequently are intolerant of variations in this parameter. Fig. 7 illustrates the spinning frequency dependence of the transfer efficiency for ^{OC}DCP in comparison to adiabatic DCP and EXPORT. However, this is not a concern as the spinning frequency is well controlled in MAS experiments, so there is no great need to be tolerant of variations in this parameter.

The magnetic field is not nearly as important a parameter as the spinning frequency in the optimization calculation. As shown in Fig. 8, pulses will typically work at lower fields as long as the spinning frequency is the same. In addition, pulses will also sometimes work at higher fields, although typically with reduced efficiency. At higher fields the pulse may not cover an adequate range of chemical shift offsets. For example, the ^{OC}DCP pulses were designed to cover a 2800 Hz (40 ppm) range of chemical shifts for ^{15}N on a 700 MHz (16.4 T) spectrometer. For a 1 GHz (23.5 T) spectrometer, this same 2800 Hz range corresponds to only 28 ppm. We do not

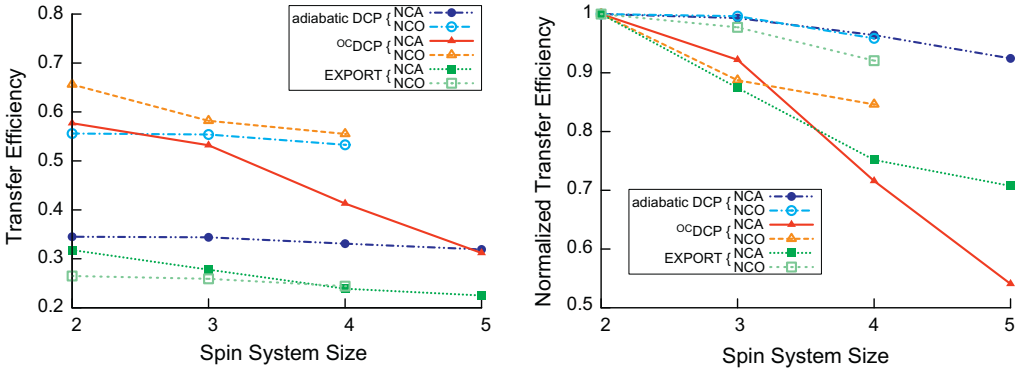

Fig. 10. Simulated NCA and NCO transfer efficiencies for adiabatic DCP, ^{OC}DCP, and EXPORT as a function of spin system size at 700 MHz for ^{1}H and with ν_r = 14 kHz. The graph to the left shows the transfer efficiencies, whereas the graph to the right shows the same data but normalized such that the two-spin result for each transfer method is set to 1.0. Filled symbols are for NCA transfers and hollow symbols are for NCO transfers. The spin systems used are illustrated in Fig. 9. The simulations used a 8% gaussian RF inhomogeneity profile.

foresee any problems in optimizing ^{OC}DCP pulses for any relevant desired field strength and spinning frequency.

Likewise, the ^{OC}DCP NCA/NCO transfer pulses were optimized while iterating over several isotropic chemical shift offsets to ensure efficient transfer over a range of chemical shifts, but only a single set of values for the ^{13}C and ^{15}N anisotropic shielding tensors was used for NCO pulses, and four values for NCA pulses. Consequently, there was no assurance that the ^{OC}DCP pulses that we calculated are tolerant of variations of the anisotropic shielding tensors or their orientations. However, it may be argued that the important issue is the frequency range invoked by the shielding parameters, independent of their origin (i.e., large anisotropies will cover smaller ones, one tensor orientation may cover others, etc.). Subsequent simulations support this view and demonstrate that all three transfer methods behave well with respect to anisotropy and asymmetry. For reasonable tensor values, the transfer efficiency rarely varies by more than 10% (see Supplementary Material).

Probably the best example of "you get what you wish for" with ^{OC}DCP pulses is how they perform in larger spin systems. As noted previously, the ^{OC}DCP pulses were calculated using a two-spin system. Although it is very computationally expensive to *optimize* pulses for larger spin systems using the current version of SIMPSON, it is possible to *simulate* the performance of these pulses in a reasonable amount of time. We created different model spin systems with between two and five spins to simulate the performance of the pulses in larger spin systems. For NCA experiments, the two-spin system consists of the amide nitrogen and the alpha carbon. Larger spin systems were constructed by adding spins for the carbonyl carbon of the preceding residue, the intraresidue carbonyl carbon, and finally the beta carbon. In the case of NCO experiments, the two-spin system consists of an amide nitrogen and the carbonyl carbon of the preceding residue. Larger spin systems were constructed by adding the intraresidue alpha carbon and then the alpha carbon of the preceding residue. These topologies are illustrated in Fig. 9. The CSA and coupling (dipolar and scalar) tensor values for these spins were calculated using SIMMOL [18] based on a poly-alanine peptide model.

Simulations of the transfer efficiencies for two, three, four, and five-spin systems are shown in Fig. 10. The results demonstrate that the ^{OC}DCP pulses are not ideally optimized for larger spin

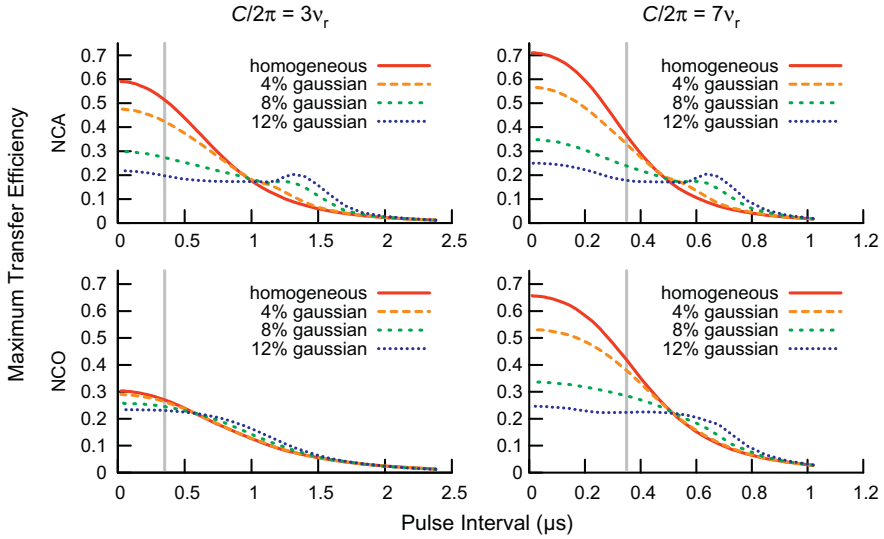

Fig. 11. Simulated NCA and NCO transfer efficiencies for EXPORT as a function of pulse interval. The results were calculated for two-spin systems at 700 MHz for ^{1}H and with ν_r = 14 kHz. The number of times the EXPORT block was repeated was optimized for each pulse interval. The left-hand graphs show results for the $C/2\pi = 3\nu_r$ condition, which is the condition used for the experimental results in this paper. The right-hand graphs correspond to the $C/2\pi = 7\nu_r$ condition, in which the average RF field strength is approximately seven times the spinning frequency. The gray vertical line indicates the smallest available pulse intervals (350 ns) for "fast" shaped pulses on our Bruker spectrometers; newer models are able to use significantly smaller pulse intervals.

systems; theoretical transfer efficiencies drop by almost half for ^{OC}DCP NCA pulses and by about 15% for ^{OC}DCP NCO pulses for the largest spin systems simulated. This effect on the transfer efficiency increases with the length of the ^{OC}DCP pulses in a roughly linear fashion (data not shown). EXPORT also suffers from decreased performance in larger spin systems relative to adiabatic DCP transfers, but the degradation is less severe than for ^{OC}DCP.

The behavior of ^{OC}DCP in the presence of additional spins explains the discrepancy between theoretical and experimental performance seen in this and previous work [10]. Additionally, this also helps explain why this discrepancy is larger for longer pulses, as seen in the middle column of Fig. 4. Simply put, for longer pulses there is more time for other dipolar couplings to interfere with the magnetization transfer. That ^{OC}DCP performs comparably or better under experimental conditions in comparison to adiabatic DCP is due to the built-in compensation for RF inhomogeneities and the limits that relaxation impose on how long the adiabatic DCP transfer period can be. Consequently, ^{OC}DCP still provides experimental transfer efficiencies higher than or equal to adiabatic DCP (Table 2 and Fig. 3) regardless of the spin systems size for NCO experiments and, for NCA experiments, ^{OC}DCP still performs comparably to adiabatic DCP even for uniformly ^{13}C,^{15}N-labeled samples.

4.3. EXPORT

EXPORT, as used in the present setup with ^{1}H decoupling, did not perform well, either theoretically or experimentally, compared to adiabatic DCP and ^{OC}DCP with respect to transfer efficiency. In addition, EXPORT is very demanding of the spectrometer hardware as it requires high RF powers and very short pulse intervals (i.e., the intervals that make up the overall pulse shape). EXPORT has the highest transfer efficiencies when using the shortest pulse intervals but is very sensitive to RF inhomogeneity under these conditions. With short pulse intervals, the transfer efficiency using an RF coil with a 8% gaussian inhomogeneity profile can be less than 50% of the efficiency using an ideal (homogeneous) RF coil. Fig. 11 illustrates how the transfer efficiency for EXPORT varies with pulse interval.

Longer pulse intervals tend to result in lower transfer efficiencies for EXPORT. Interestingly, as the pulse intervals become longer, there is a regime where the transfer is robust with respect to RF inhomogeneity and, for even longer pulse intervals there can even be a regime where the transfer efficiency *improves* with increasing RF inhomogeneity. Unfortunately, this behavior with respect to RF inhomogeneity does not fully counter the drop in transfer efficiency when using longer pulse intervals. Regardless of the amount of RF inhomogeneity, the best transfer efficiencies are achieved with the shortest possible pulse intervals.

In this paper, we used the $C/2\pi = 3\nu_r$ condition for EXPORT, which results in average RF fields of around 42 kHz for the ^{15}N and ^{13}C channels when using a sample spinning frequency of 14 kHz. However, a higher power condition ($C/2\pi = 7\nu_r$) has also been described [11]. This condition is experimentally inaccessible on our 3.2 and 4 mm probes as it requires RF amplitudes of around 98 kHz for each channel when spinning the sample at 14 kHz. Nevertheless, we simulated the performance of EXPORT using the $C/2\pi = 7\nu_r$ condition to see if this would result in a better outcome relative to the $C/2\pi = 3\nu_r$ condition. As shown on the right in Fig. 11, the higher amplitude condition improves the transfer efficiency if the RF field is relatively homogeneous. Under conditions similar to our experimental conditions (350 ns pulse intervals, 8% gaussian RF inhomogeneity), the transfer efficiency using the $C/2\pi = 7\nu_r$ condition is slightly better for NCO but slightly worse for NCA compared to EXPORT transfers using the $C/2\pi = 3\nu_r$ condition. For the conditions of 50–100 ns digitization (as can be achieved with newer spectrometer consoles), the transfer efficiency is always better for the higher power condition but is also more susceptible to RF inhomogeneities.

5. Conclusions

For moderate spinning frequencies (10–20 kHz), adiabatic DCP and ^{OC}DCP tend to have similar efficiencies for ^{15}N–^{13}C transfers. Which method works best depends on the nature of the sample and the probe; systems with more homogeneous RF fields favor adiabatic DCP transfers, while samples with non-uniform labeling schemes favor ^{OC}DCP transfers. Further advantages of ^{OC}DCP pulses are that they require less power for shorter periods of time (so they are more suitable for sensitive samples) and that they are much more robust with respect to RF inhomogeneity and RF power levels (which makes them easier to calibrate and better suited for long experiments where the instrument conditions may drift with time). EXPORT transfers did not perform well under the conditions investigated, but may be better suited at the high ^{15}N/^{13}C RF power conditions for which they were originally proposed and where efficient transfers may be achieved without ^{1}H decoupling.

Acknowledgments

Thanks to Anne Diehl and Matthias Hiller (FMP-Berlin) for their help preparing samples and to Jochem Struppe and Hans Förster at Bruker Biospin for useful conversations. We acknowledge support from the Danish National Research Foundation and the Danish Center for Scientific Computing. N.M.L. was supported by Award Number R15GM085733 from the National Institute of General Medical Sciences.

Appendix A. Supplementary material

SIMPSON scripts for generating and testing ^{OC}DCP pulses as well as shape files (in Bruker format) for all pulses (^{OC}DCP, EXPORT, and adiabatic DCP) at both spinning frequencies (12 and 14 kHz) are provided in the supplementary information as well as at: http://lclark.edu/~loening/pulses.html. Supplementary data associated with this article can be found, in the online version, at doi:10.1016/j.jmr.2011.10.012.

References

[1] J. Schaefer, E. Stejskal, J. Garbow, R. McKay, Quantitative determination of the concentrations of ^{13}C–^{15}N chemical bonds by double cross-polarization NMR, J. Magn. Reson. 59 (2003) 150–156.
[2] G. Metz, X.L. Wu, S.O. Smith, Ramped-amplitude cross polarization in magic-angle-spinning NMR, J. Magn. Reson., Ser. A 110 (1994) 219–227.
[3] M. Baldus, D.G. Geurts, S. Hediger, B.H. Meier, Efficient ^{15}N–^{13}C polarization transfer by adiabatic-passage Hartmann-Hahn cross polarization, J. Magn. Reson., Ser. A 118 (1996) 140–144.
[4] M. Baldus, A.T. Petkova, J. Herzfeld, R.G. Griffin, Cross polarization in the tilted frame: assignment and spectral simplification in heteronuclear spin systems, Mol. Phys. 95 (1998) 1197–1207.
[5] M. Bjerring, N.C. Nielsen, Solid-state NMR heteronuclear coherence transfer using phase and amplitude modulated rf irradiation at the Hartmann-Hahn sideband conditions, Chem. Phys. Lett. 382 (2003) 671–678.
[6] Y.K. Lee, N.D. Kurur, M. Helmle, O.G. Johannessen, N.C. Nielsen, M.H. Levitt, Efficient dipolar recoupling in the NMR of rotating solids: a sevenfold symmetric radiofrequency pulse sequence, Chem. Phys. Lett. 242 (1995) 304–309.
[7] A. Brinkmann, M.H. Levitt, Symmetry principles in the nuclear magnetic resonance of spinning solids: heteronuclear recoupling by generalized HartmannHahn sequences, J. Chem. Phys. 115 (2001) 357–384.
[8] M. Bjerring, N.C. Nielsen, Solid-state NMR heteronuclear dipolar recoupling using off-resonance symmetry-based pulse sequences, Chem. Phys. Lett. 370 (2003) 496–503.
[9] C.T. Kehlet, A.C. Sivertsen, M. Bjerring, T.O. Reiss, N. Khaneja, S.J. Glaser, N.C. Nielsen, Improving solid-state NMR dipolar recoupling by optimal control, J. Am. Chem. Soc. 126 (2004) 10202–10203. PMID: 15315406.
[10] C. Kehlet, M. Bjerring, A.C. Sivertsen, T. Kristensen, J.J. Enghild, S.J. Glaser, N. Khaneja, N.C. Nielsen, Optimal control based NCO and NCA experiments for

spectral assignment in biological solid-state NMR spectroscopy, J. Magn. Reson. 188 (2007) 216–230.
[11] A.B. Nielsen, L.A. Straasø, A.J. Nieuwkoop, C.M. Rienstra, M. Bjerring, N.C. Nielsen, Broadband heteronuclear solid-state NMR experiments by exponentially modulated dipolar recoupling without decoupling, J. Phys. Chem. Lett. 1 (2010) 1952–1956.
[12] L.S. Pontryagin, V.G. Boltyanskii, R.V. Gamkrelidze, E.F. Mishchenko, The Mathematical Theory of Optimal Processes, Wiley-Interscience, New York, 1962.
[13] A.E. Bryson, Jr., Y.-C. Ho, Applied Optimal Control: Optimization, Estimation, and Control, Hemisphere, Washington, DC, 1975.
[14] N.C. Nielsen, C. Kehlet, S.J. Glaser, N. Khaneja, Optimal control methods in NMR spectroscopy, in: R.K. Harris, R.E. Wasylishen (Eds.), Encyclopedia of Magnetic Resonance, John Wiley & Sons, Ltd, 2010.
[15] M. Bak, J.T. Rasmussen, N.C. Nielsen, SIMPSON: a general simulation program for solid-state NMR spectroscopy, J. Magn. Reson. 147 (2000) 296–330.
[16] Z. Tosner, T. Vosegaard, C. Kehlet, N. Khaneja, S.J. Glaser, N.C. Nielsen, Optimal control in NMR spectroscopy: numerical implementation in SIMPSON, J. Magn. Reson. 197 (2009) 120–134.
[17] M. Bak, N.C. Nielsen, REPULSION, a novel approach to efficient powder averaging in solid-state NMR, J. Magn. Reson. 125 (1997) 132–139.
[18] M. Bak, R. Schultz, T. Vosegaard, N.C. Nielsen, Specification and visualization of anisotropic interaction tensors in polypeptides and numerical simulations in biological solid-state NMR, J. Magn. Reson. 154 (2002) 28–45.
[19] J. Pauli, B. van Rossum, H. Förster, H.J.M. de Groot, H. Oschkinat, Sample optimization and identification of signal patterns of amino acid side chains in 2D RFDR spectra of the [alpha]-spectrin SH3 domain, J. Magn. Reson. 143 (2000) 411–416.
[20] M. Hiller, V.A. Higman, S. Jehle, B.-J. van Rossum, W. Kühlbrandt, H. Oschkinat, [2,3-^{13}C]-labeling of aromatic residues–getting a head start in the magic-angle-spinning NMR assignment of membrane proteins, J. Am. Chem. Soc. 130 (2008) 408–409.
[21] B.M. Fung, A.K. Khitrin, K. Ermolaev, An improved broadband decoupling sequence for liquid crystals and solids, J. Magn. Reson. 142 (2000) 97–101.